Supporting Information

In-situ synthesis of dispersed borides induced high-performance brazed DD5 superalloy via a novel sandwich-structured interlayer

Fushuai Jin, Jilong Wang, Wenhao Wang, Zhiwei Qin*, Yutao Sun, Xiaolong Hong, Yu Zhou, Jingkuan Wang, Peng Li, Shuyan Shi, Honggang Dong[1]*

School of Materials Science and Engineering, Dalian University of Technology, Dalian 116024, PR China

* Corresponding author: E-mail: qinzw@dlut.edu.cn, donghg@dlut.edu.cn

[1]* **Corresponding author.**
E-mail address: donghg@dlut.edu.cn (Honggang Dong), Tel: +86-411-84706283.

Table of contents

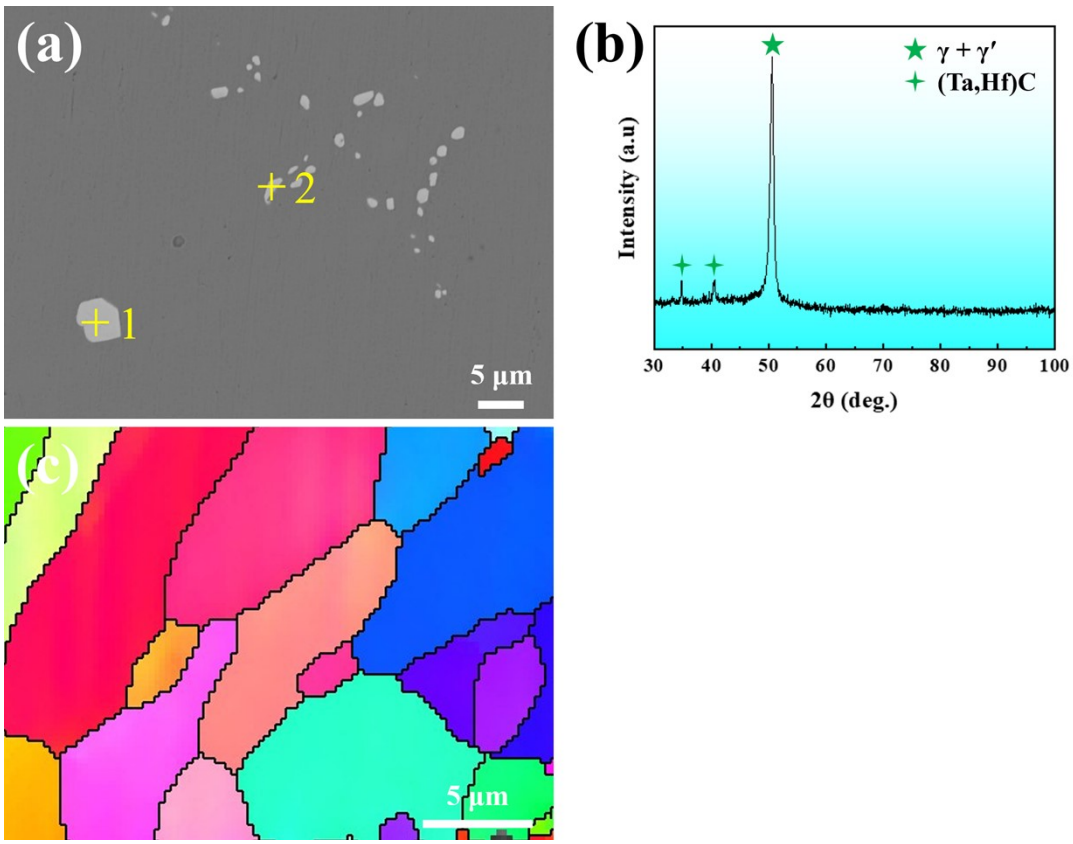

Figure S1. Microstructural and crystallographic characterization. (a) Microstructure of the DD5 base metal. (b) XRD pattern of the DD5 alloy. (c) Inverse pole figure (IPF) map of the NiCrWMoAlRe interlayer.

Table S1. Elemental results of the EPMA points at the marked positions in Supplementary Figure 1 (at.%).

Point	Ni	Co	Al	Cr	W	Mo	Ta	Hf	Re	C
1	4.42	0.93	0	1.33	3.48	1.36	41.56	4.64	0	41.19
2	20.65	2.66	4.59	3.00	2.60	0.67	36.61	3.29	0.27	24.88

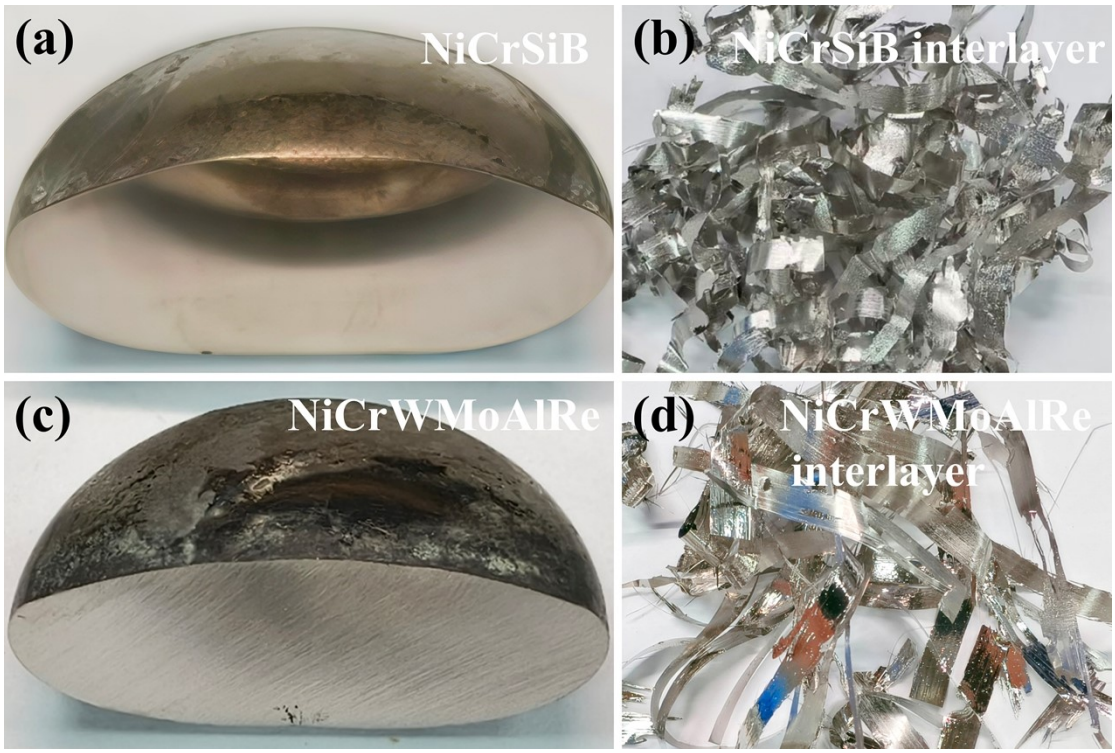

Figure S2. Morphologies of metal ingots and foils. (a) Metal ingot and (b) foil morphology of NiCrSiB; (c) Metal ingot and (d) foil morphology of NiCrWMoAlRe.

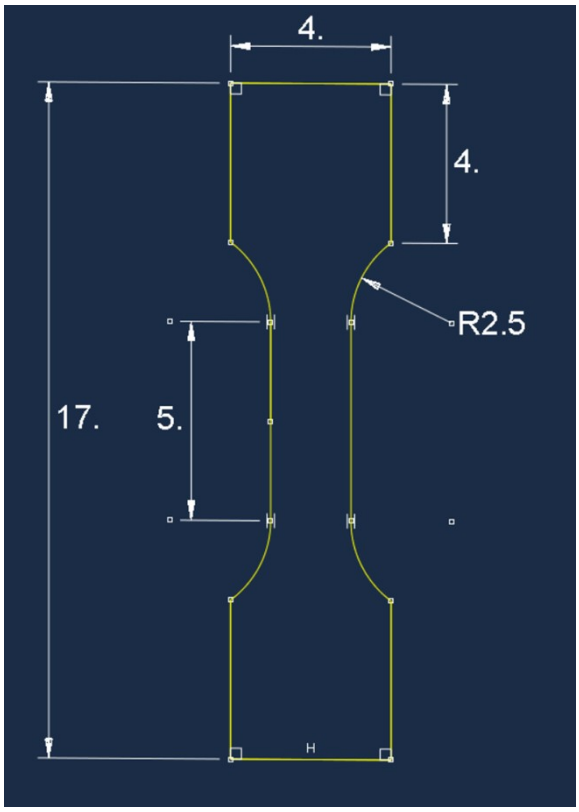

Figure S3. Dimensions of tensile test specimens (unit: mm)

Table S2. Chemical compositions of the EPMA points at the marked positions in Fig. 2 (at.%).

Point	Ni	Cr	W	Mo	B	Si	Ta	Al	Possible Phase
1	16.13	24.85	6.25	4.62	38.30	0.51	0.34	0.76	Cr/Mo/W-rich borides
2	23.89	27.87	2.79	1.64	30.95	1.31	0.12	1.93	Cr/Mo/W-rich borides
3	74.28	8.90	0.54	0.18	0	4.75	0.56	4.32	$\gamma + \gamma'$
4	76.47	4.99	0.27	0.10	8.34	0.41	1.94	3.06	Ni-Si-B eutectic
5	75.96	8.56	0.29	0.14	0	8.61	0.09	2.12	
6	46.66	15.82	2.03	2.21	23.44	2.44	0.23	3.95	Cr/Mo/W-rich borides
7	14.40	40.77	5.38	7.28	26.99	0	0	0.09	Cr/Mo/W-rich borides
8	77.0	4.85	0.17	0.11	7.64	0.20	1.26	4.48	Ni-rich borides
9	30.62	22.55	3.81	10.24	27.22	1.02	0	1.64	Cr/Mo/W-rich borides
10	72.03	8.30	1.84	2.42	0.05	2.28	0	8.86	-
11	75.55	8.79	0.44	0.28	0	3.90	0.32	6.07	$\gamma + \gamma'$
12	77.16	7.43	0.52	0.21	0	4.78	0.40	7.67	$\gamma + \gamma'$

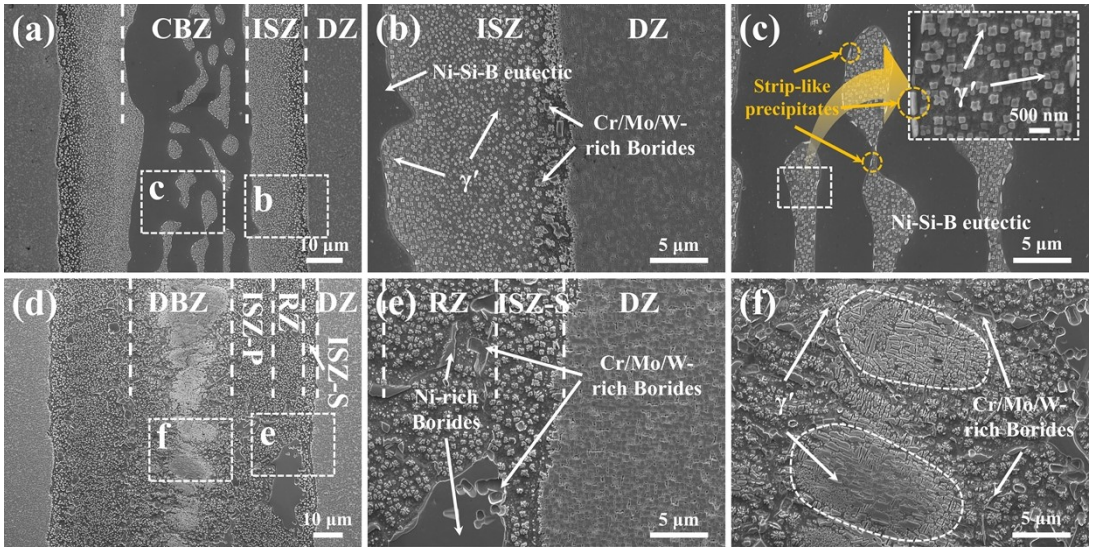

Figure S4. Microstructure of precipitated phase of the joints. (a) The microstructure of overall SC-joint. (b) The microstructure of ISZ and DZ. (c) The microstructure of CBZ. (d) The microstructure of overall SS-joint. (e) The microstructure of RZ, ISZ-S and DZ. (f) The microstructure of DBZ.

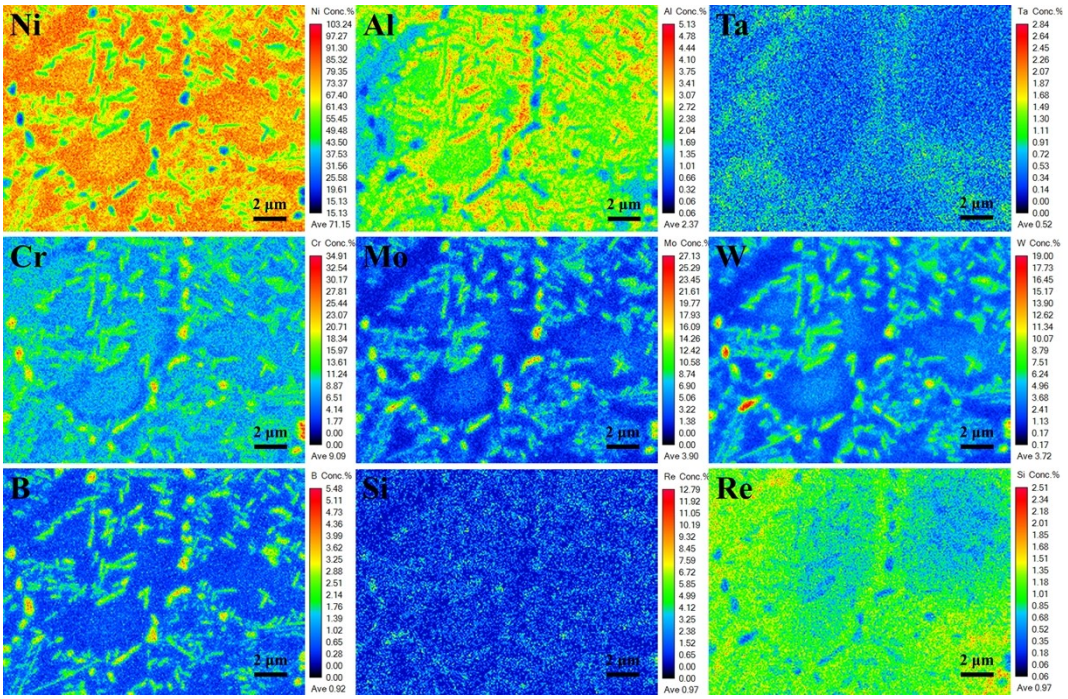

Figure S5. Elements mapping results of Figure 2f.

Table S3. Comparison of welding processes

	This work	Si/B-free fillers	Partial TLP	Mortise-tenon structures
Parameters	1100 °C for 20 min	1200°C for 30 min	1260°C for 60 min	1280°C for 60 min
Key microstructural features	Dispersed Boride Zone	No borides	Epitaxial Growth Zone	Polycrystalline Joint
Complexity	Moderate	Moderate	Precise	Very High

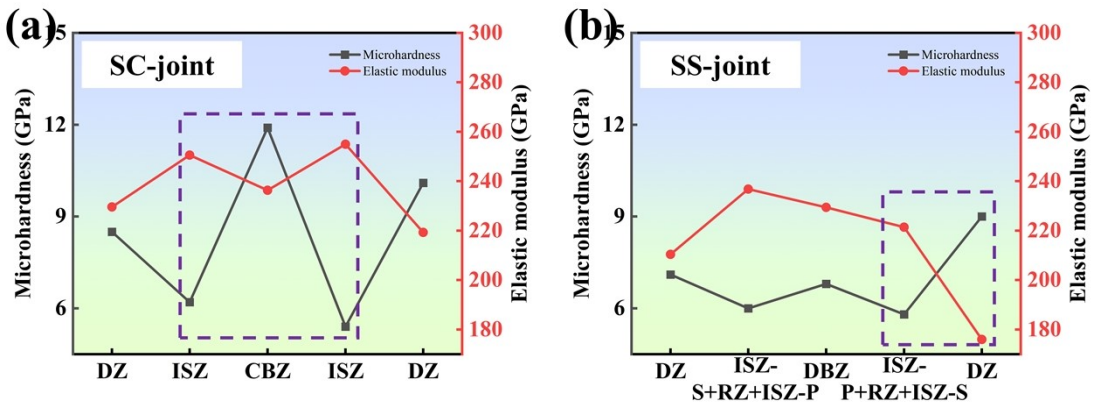

Figure S6. Nanoindentation results across different regions of the joints. (a) SC-joint. (b) SS-joint.

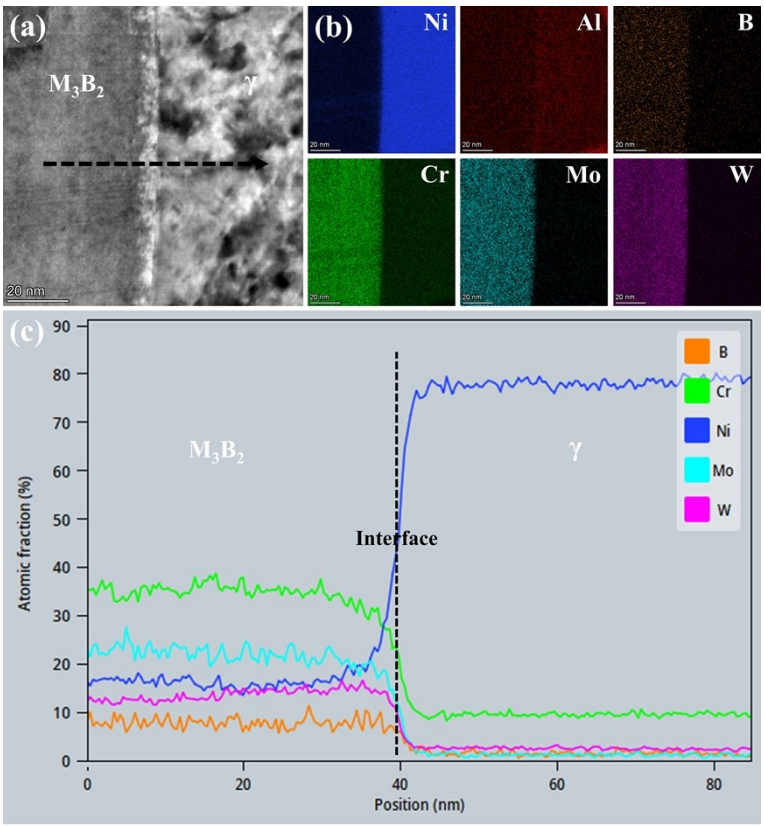

Figure S7. TEM analysis of the M_3B_2/γ interface. (a) A bright-field TEM image. (b) STEM-EDS mapping corresponding to each element of the region in (a). (c) Line scan results in (a)

Table S3. The formation enthalpy (ΔH_f) for all studied binary borides[1]

Phase	ΔH_f	Phase	ΔH_f	Phase	ΔH_f
$Cr_{23}B_6$	-17.47	$Mo_{23}B_6$	-18.47	$W_{23}B_6$	-15.74
Cr_3B	-17.26	Mo_3B	-23.62	W_3B	-17.26
Cr_5B_3	-47.87	Mo_5B_3	-42.31	W_5B_3	-31.96
Cr_3B_2	-49.42	Mo_3B_2	-45.68	W_3B_2	-33.96
CrB	-59.99	MoB	-58.31	WB	-43.79

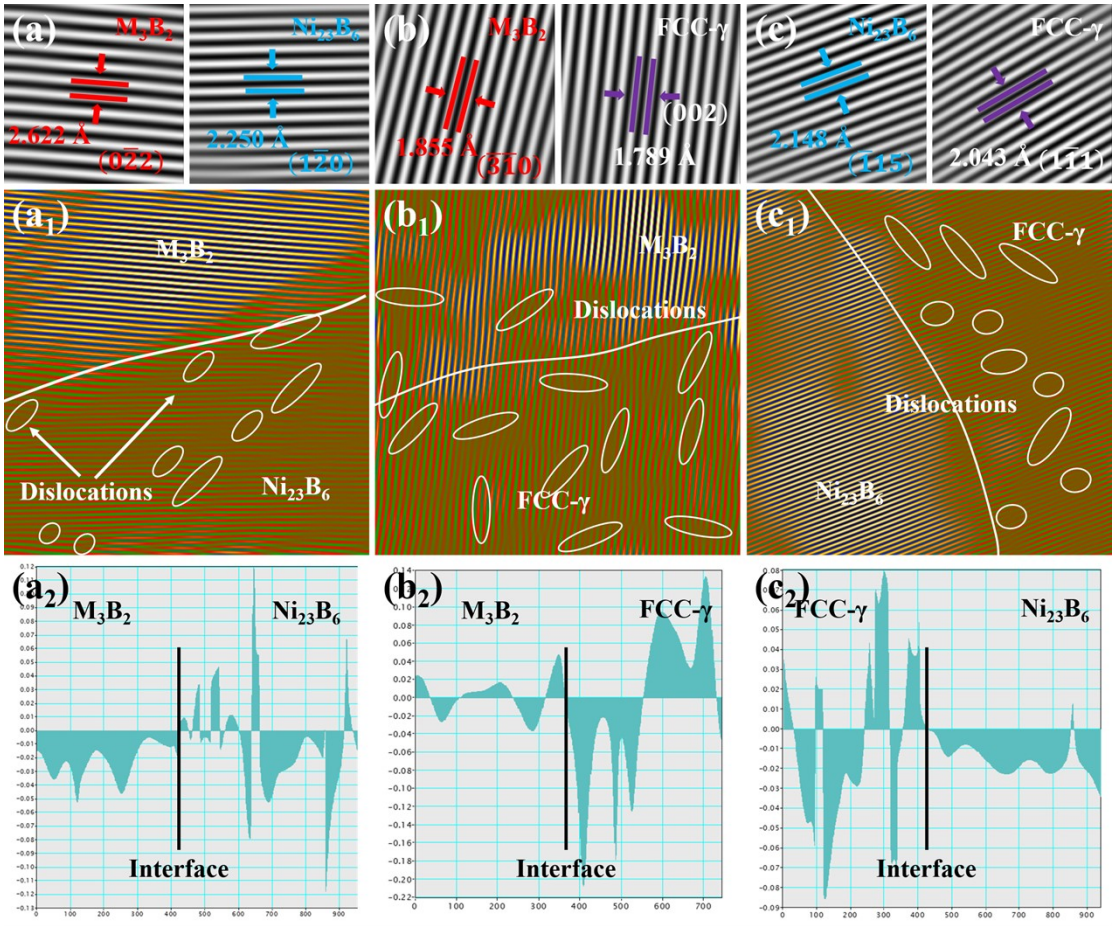

Figure S8. Nanoindentation results across different regions of the joints. (a) SC-joint. (b) SS-joint.

References

1 H. K. Zhang, J. S. Chen, L. X. Zhang, et al., *Phase Transitions*, 2020, 93, 158–174, DOI:10.1080/01411594.2019.1692015.